Combined Axial Pressure and Screening Current Induced Stress Test on REBCO Pancake Coils

Yu Suetomi, Kwangmin Kim, Todd Adkins, Hongyu Bai, and Iain R. Dixon, *Senior Member, IEEE*

***Abstract*—Screening current induced stress (SCIS) causes conical deformation in REBCO pancake coils. In an actual ultra-high field magnet, a REBCO pancake coil is subjected to axial pressure from upper pancake coils, in addition to SCIS. This axial pressure likely enhances the conical deformation and hoop strain. In this study, we developed a test scheme, referred to as the combined axial pressure and tape tilting (CATT) test, to investigate the degree of strain enhancement caused by axial pressure. As a result of the test, a 50% increase of hoop strain was observed at an axial load of 180 kN, leading to yielding of the REBCO tapes. Buckling deformation due to compressive hoop strain was also observed during the charging test with current in negative direction under a background field.**

***Index Terms*—Axial pressure, REBCO coil, screening current induced stress, ultra-high field superconducting magnet.**

I. Introduction

SCREENING current induced stress (SCIS) is becoming a significant issue for ultra-high field (UHF) magnets utilizing REBCO tapes [1], [2], [3], [4], [5], [6], [7], [8], [9]. The screening currents in REBCO tapes generate outward and inward Lorentz forces, leading to conical deformation of the REBCO pancake coil with tilting of the REBCO tapes, enhancement of tensile hoop strain, and the occurrence of compressive hoop strain. This can results in excessive tensile hoop stress, which can cause yielding [2], [8], [10], while compressive hoop stress may lead to buckling deformation [6]. Although yielding due to excessive hoop stress is well studied, buckling due to compressive hoop stress and influences of the tilting angle of REBCO tapes is not well understood. Our previous work reported that large-diameter coils, such as the outer REBCO coil in a UHF magnet, tend to experience significant compressive hoop strain and tilting angle [9].

On the other hand, another challenge for REBCO coils in UHF magnets is the large axial pressure near the mid-plane region, caused by the accumulation of Lorentz force from the upper regions. Some studies have reported the tolerance of REBCO pancake coils to axial pressure [11], [12], [13]. A pancake coil wound by a single REBCO tape was degraded around 100 MPa, while a multi-tape wound REBCO pancake coil demonstrated a tolerance of >125 MPa of axial pressure [13].

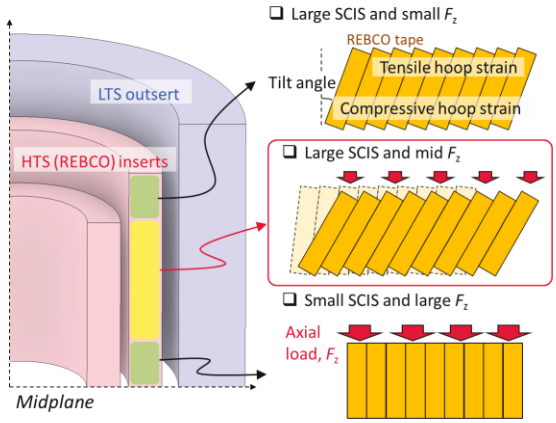

Fig. 1. Challenges in UHF magnet and focus of this study: The combination of axial pressure and screening current induced stress (SCIS).

The SCIS and tolerance to axial pressure have been studied individually; however, in an actual coil, they occur simultaneously, particularly in the mid-region of the outer REBCO coil. This region is likely subjected to both significant SCIS and moderate axial pressure. One role of axial pressure is to provide frictional forces between the coil's top and bottom surface and spacers inserted between pancake disks, which suppress radial movement of the tapes caused by Lorentz forces, thereby reducing hoop strain [1], [14]. On the other hand, axial pressure may also increase the magnitude of conical deformation and hoop strain, as illustrated in Fig. 1. In this context, a larger tilt angle could lead to greater hoop strain enhancement due to axial pressure, resulting in degradation of the REBCO tapes. Currently, there is no evidence to support this hypothesis, necessitating experimental investigation.

In this study, we developed a new test scheme and investigated the degree of strain enhancement due to axial pressure and resulting degradation.

II. Test Setup and Procedure

Fig. 2(a) illustrates the design of the test setup, consisting of a 12 T-LTS split magnet with 150 mm clear bore, a REBCO double pancake coil, and a 250 kN hydraulic actuator attached

Received 25 September 2024; revised 27 November 2024; accepted 12 December 2024. Date of publication 23 December 2024; date of current version 3 January 2025. This work was supported in part by the National Science Foundation Cooperative under Agreement DMR-2131790 and Agreement DMR-2128556 and in part by the State of Florida. This work was performed at the National High Magnetic Field Laboratory. *(Corresponding author: Yu Suetomi.)*

The authors are with National High Magnetic Field Laboratory, Florida State University, Tallahassee, FL 32310 USA (e-mail: yu.suetomi@magnet.fsu.edu).

Color versions of one or more figures in this article are available at https://doi.org/10.1109/TASC.2024.3520943.

Digital Object Identifier 10.1109/TASC.2024.3520943

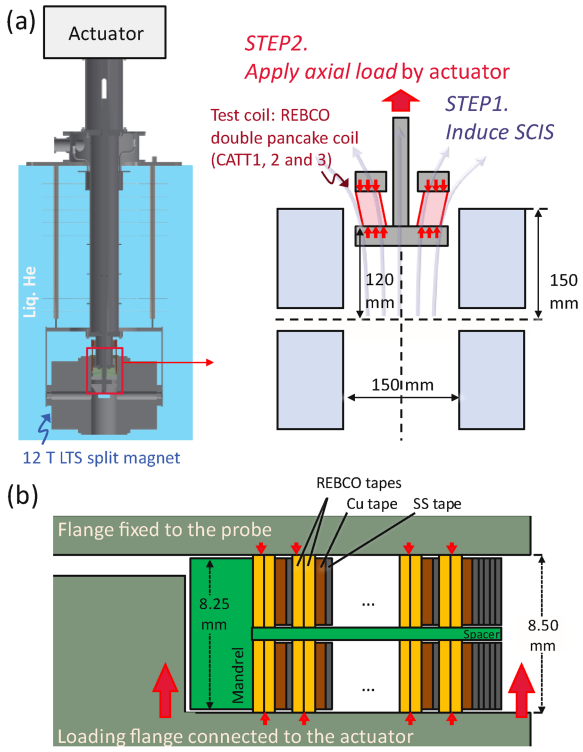

Fig. 2. (a) Schematic of the test setup. (b) Schematic cross-section of CATT 1.

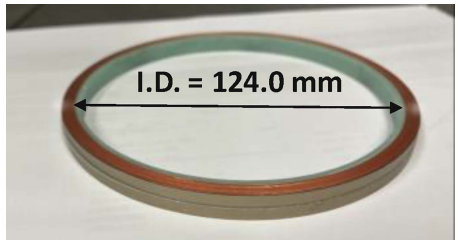

Fig. 3. Photo of CATT 1 before attaching terminals.

TABLE I
SPECIFICATIONS OF TEST COILS

	CATT 1	CATT 2	CATT 3
I.D. / O.D. [mm]	124.0 / 131.3		
Components of a turn and its thickness	REBCO tape (Cu: 40 μm, Hastelloy: 50 μm) x 2 Cu tape: 127 μm x 1 Insulated stainless-steel tape: 50 μm x 1		
Total turns	20 turns (10 turns x 2 pancakes)		
Over-band thickness	50 μm x 4 turns	50 μm x 1 turns	50 μm x 1 turns
Mandrel material	G-10	G-10	Stainless-steel
Impregnation	None	Wax	Wax

to the top of the probe. The REBCO coil is positioned 120 mm axially away from the mid-plane of the background magnet where the center of the cross-section of the test coil experiences a magnetic field with an angle of 11° to the z-axis. The test scheme consists of two main steps. Step 1: the background magnet, and in some cases the test coil, is charged to induce screening currents, generating SCIS and causing tilting deformation in the test coil. Step 2: axial load is applied to the REBCO coil using the actuator while maintaining the charging current, meaning axial pressure is applied while the REBCO pancake coil remains conical deformation due to SCIS. This test is referred to as the combined axial pressure and tape tilting (CATT) test. This CATT test can imitate the stress and strain conditions in the mid-region of a UHF magnet as illustrated in Fig. 1. Although the SCIS and axial pressure are applied simultaneously in actual conditions, in this experiment, axial pressure is applied after inducing SCIS to focus on the strain enhancement caused by axial pressure.

For this test, we fabricated three double pancake REBCO coils, named CATT 1, CATT 2 and CATT 3 (see Fig. 3), with their parameters listed in Table I. Each coil has an inner diameter of 124.0 mm, an outer diameter of 131.3 mm and a total 20 turns. These coils do not have an inner joint at the inner diameter. Each turn consists of four tapes: two REBCO tapes, a Cu tape and an insulated stainless-steel (SS) tape. Additionally, the coils have an over-banding (OB) by winding SS tape. The REBCO tapes used for winding CATT 1, 2 and 3 were all extracted from the same spool. CATT 1 has a total OB thickness of 200 μm, while CATT 2 and CATT 3 have a less OB thickness of 50 μm. The mandrel material differs between coils: G-10 for CATT 1 and 2, and insulated SS for CATT 3. Details about the insulation coating are provided in [15]. Fig. 2(b) shows a schematic cross-section of CATT 1. The upper flange is fixed to the probe, while the lower flange is connected to the actuator via a rod. The mandrel is designed as 0.25 mm shorter than the total height of winding pack, and the co-wound Cu and SS tapes are narrower than the REBO tape. Thus, when the lower flange is moved upward by the actuator, the axial pressure is applied only to the REBCO tapes.

Before the test, we predicted the strain and tilting angle due to SCIS using numerical simulation to define the test condition. The details of the simulation model are described in [9]. The structural geometry was discretized for each REBCO, Cu, SS tapes and mandrel. The mandrel is common for both upper and lower pancake disks. The mandrel and co-wound tapes have the same height as the total height of the winding pack and the height of the REBCO tape, respectively, for ease of calculation. A roller-corner condition was applied to the outward-bottom corner of each geometry, constraining displacement in the z-axis direction to be zero. The interface between each geometry is modeled with frictionless contact using a penalty method. Although this simulation model assumes only elasticity, we account for the large deformation caused by plasticity in the co-wound Cu tape by using an effective modulus derived from measured stress at 0.5% strain point after yielding. For the I_c calculation, we used the formula introduced by Jaroszynski [16], with parameters fitted to the measured I_c-θ curve at $T = 4.2$ K

TABLE II
OPERATING CONDITIONS

Operating conditions		CATT1	CATT2	CATT3
Step 1:	Background field	9.1 T / 11°	9.6 T / 11°	6.9 T / 11°
	Test coil current	0 A	0 A	502 A
	Simulated values			
	Max. tape tilt angle	9.0°	9.4°	5.8°
	Max. hoop strain on REBCO tapes	0.54%	0.57%	0.43%
Step 2:	Axial load (Averaged axial pressure*)	120 kN (82 MPa)	120 kN (82 MPa)	180 kN (122 MPa)
	Fatigue cycle number (load range)	20k (10–120 kN)	5k (10–90 kN) 15k (10–120 kN)	20k (20–170 kN)
Step 3:	Background field	9.1 T / 11°	-	9.6 T / 11°
	Target current for test coils	−1.2 kA (~90% to I_c)	-	−1.2 kA (~94% to I_c)

*Averaged to the surface area of the test coil

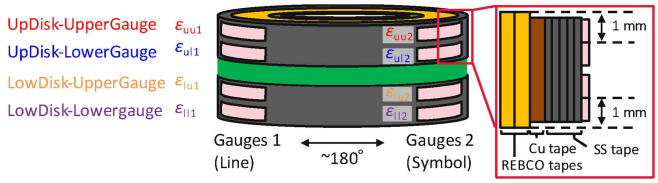

Fig. 4. Schematic of the attached strain gauges.

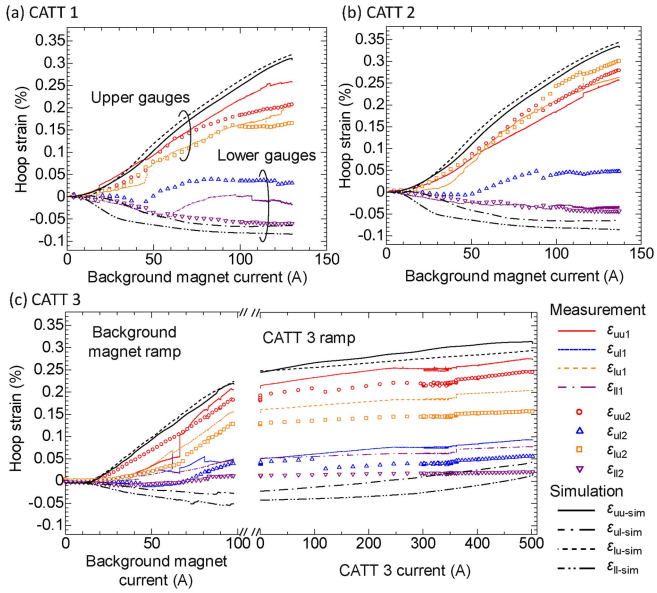

Fig. 5. Measured strain during step 1 in (a) CATT 1, (b) CATT 2 and (c) CATT 3, compared with simulated hoop strain by numerical simulation.

and $B = 9$, 12 and 14 T for the REBCO tape used in CATT 1, 2 and 3.

Table II summarizes the operating condition of CATT test for CATT 1, 2 and 3. During the test, we measured coil voltage and hoop strain using strain gauges. A total of eight strain gauges (ε_{uu1}, ε_{ul1}, ε_{lu1}, ε_{ll1}, ε_{uu2}, ε_{ul2}, ε_{lu2} and ε_{ll2}) were attached to the surface of the outermost over-band tape, as shown in Fig. 4. In this paper, we refer to the strain gauges attached to the upper halves ("UpperGauge" in Fig. 4) and lower halves ("LowerGauge" in Fig. 4) of the pancake disk as "upper gauges" and "lower gauges", respectively. Each strain gauge is positioned approximately 90° from the terminal joint locations. The gauges were zeroed after cooldown and the strain gauge signal were calibrated using a compensation gauge installed near the coil.

III. TEST RESULTS AND DISCUSSIONS

Step 1. Induce SCIS and tape tilting deformation: Fig. 5 shows the measured hoop strain during step 1 in (a) CATT 1, (b) CATT 2 and (c) CATT 3. After cooldown to 4.2 K, the background magnet was charged to 130 A for CATT 1, producing 9.1 T with 11° for the coil, and to 137 A for CATT 2, resulting 9.6 T with 11°. In the case of CATT3, the background magnet was charged to 98 A, while CATT 3 was charged to 502 A. This operation aimed to create a relatively small tape tilting angle while maintaining a large hoop strain. These operating conditions are summarized in Table II.

The results for CATT 1, 2 and 3 indicate that the upper gauges exhibit larger strains than the lower gauges, confirming the expected tape tilting deformation due to SCIS. The figures also reveal that the deformation was not uniform in circumferential direction. There is approximately 20% difference between ε_{uu1} and ε_{uu2} in CATT 1. This is likely due to the presence of the turn's tail-end and terminal joint. Comparing CATT 1 and 2, the upper gauges of CATT 2 show larger strain than those of CATT 1, attributed to the less over-band thickness in CATT 2. Additionally, some lower gauges, such as ε_{ul2} and ε_{ll1} in CATT 1, exhibit sudden changes in trend of strain. This is likely because these gauges were attached to the outermost over-band, which was less sensitive to inward Lorentz forces and more influenced by the contact state between the tape edge and the flange or spacer.

The simulated hoop strain at the gauge location is also shown in Fig. 5 with black solid ($\varepsilon_{uu\text{-}sim}$), dashed ($\varepsilon_{lu\text{-}sim}$), single-pointed ($\varepsilon_{ul\text{-}sim}$) and double-pointed ($\varepsilon_{ll\text{-}sim}$) lines. The simulation results for all coils generally match the measurements, although the simulated strain are approximately 20% larger. The reason for this discrepancy remains uncertain and requires

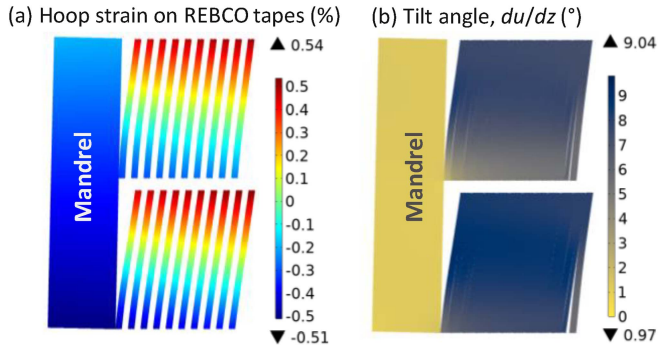

Fig. 6. Simulated distribution of (a) hoop strain on REBCO tapes and (b) tilt angle of CATT 1 after charging the background magnet.

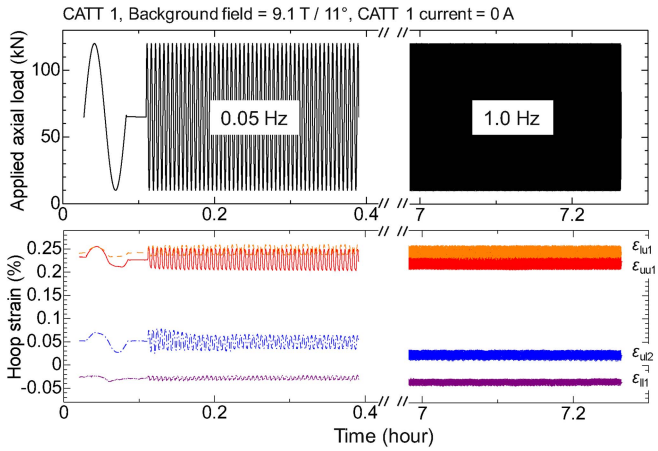

Fig. 7. Applied axial load and measured hoop strain during fatigue cycles in CATT 1.

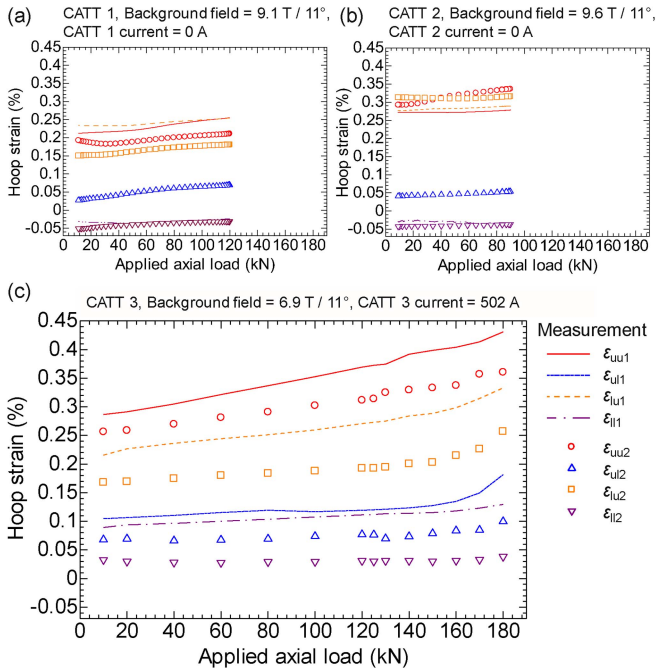

Fig. 8. Relationship between measured hoop strain and applied axial load for (a) CATT 1, (b) CATT 2, and (c) CATT 3.

further investigation. Fig. 6 displays the simulated hoop strain on REBCO tape and tilt angle distribution in CATT 1 after charging the background magnet to 9.1 T. The maximum values are 0.54% for hoop strain and 9.0° for tilting angle. Table II also summarizes the simulated maximum hoop strain and tilt angles for CATT 1, 2 and 3. As noted, CATT 3 had a smaller simulated tilt angle of 5.8° as expected.

As the result of step 1, we created the intended tilt angle and hoop strain in CATT 1, 2 and 3, although the actual magnitude are likely somewhat lower than those listed in Table II.

Step 2. Apply axial load and fatigue cycles: Axial loads were applied to the coils using the actuator, while maintaining the current to preserve the tilting deformation caused by SCIS. A total of 20,000 axial load cycles within the load range described in Table II were also applied to assess the effects of fatigue. Understanding the fatigue life of the coil is crucial for user magnets, as they undergo numerous charge-discharge cycles and experience repeated loading from Lorentz force. Load cycles were applied with a sine wave at frequencies between 0.005–1.0 Hz. The maximum applied axial loads were 120 kN for CATT 1 and 2, and 180 kN for CATT3, corresponding to average axial pressures of 82 and 122 MPa on the coil's surface, respectively. Fig. 7 displays the applied axial load and measured hoop strain during fatigue cycles in CATT 1. The measured strain correlates with the applied axial load.

Fig. 8(a), (b) and (c) shows the relationship between measured hoop strain and applied axial load for CATT 1, 2 and 3, respectively. The results were extracted from data during the first load cycle. Fig. 9 compares hoop strain enhancement at the gauge ε_{uu1} by axial load in CATT 1, 2 and 3. The strain was normalized to the hoop strain at 10 kN. Results for CATT 3 clearly demonstrate that the measured hoop strain was enhanced by the axial load, with ε_{uu1} increasing by 50% due to the axial load of 180 kN. CATT 3 also shows greater strain enhancement than the other coils, contrary to our initial conjecture that a larger tilt angle would result in greater strain enhancement. The smaller strain enhancement in CATT 1 and 2 might be attributed to the mandrel receiving some axial loads due to large tilt angle. Tilting deformation reduces the level of the coil's top surface and raises the level of the mandrel's inner-upper edge, as shown in the simulated deformation in Fig. 6. Although the mandrel was shorter than the winding pack, it might have been insufficient. Therefore, the actual axial pressure the coil was subjected to is uncertain. Improvements are needed in future work to accurately quantify the applied axial pressure.

During fatigue cycle, the relationship between measured strain and axial load remained nearly constant. For CATT 2, the maximum axial load was increased from 90 to 120 kN after confirming that there were no significant strain changes during 5000 load cycles. Also, since we observed nonlinear strain increases on some gauges during initial increase of axial

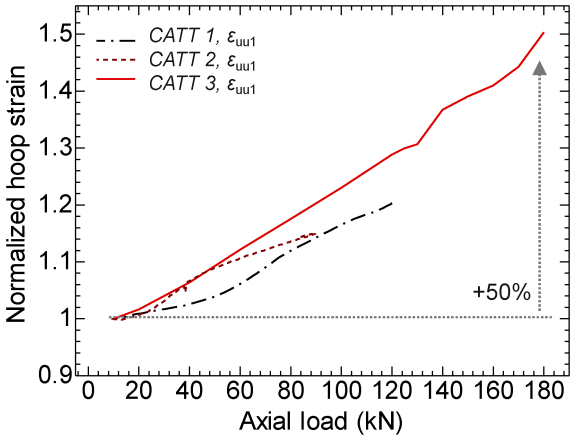

Fig. 9. Comparison of measured hoop strain for CATT 1, CATT 2, and CATT 3. The strain is normalized to the value at 10 kN of axial load.

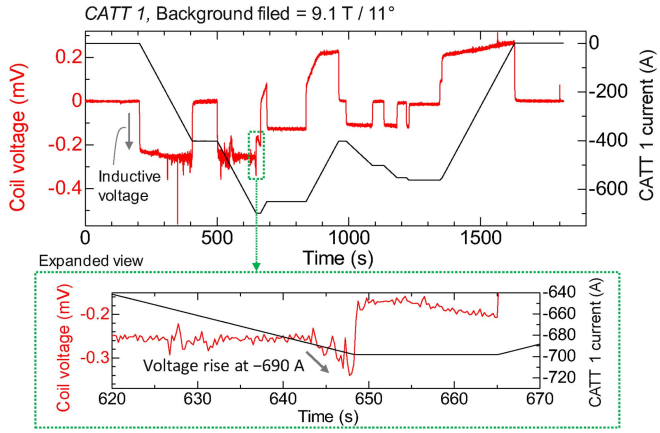

Fig. 10. Test results of negative current operation in CATT 1.

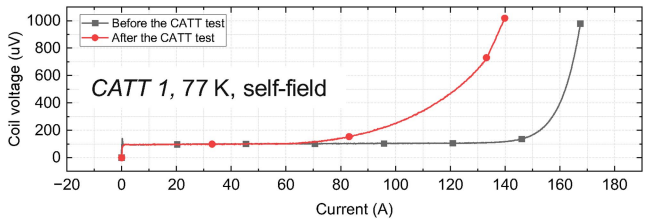

Fig. 11. Voltage-current curve of CATT 1 at 77 K under self-filed.

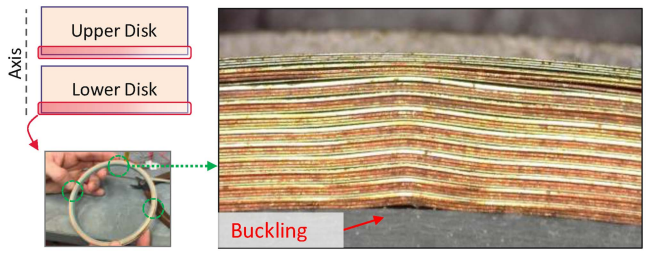

Fig. 12. Buckling found on CATT 1 after the test.

load in CATT 3, as shown in Fig. 8(c), the fatigue cycle for CATT 3 was performed within a load range from 20 to 170 kN.

Step 3. Evaluate the coil performance and degradation: After the fatigue test, we evaluated the coil performance through a charging test at 4.2 K under background field, a charging test at 77 K under self-field, visual inspection, and measurement of the I_c distribution in the longitudinal direction of the REBCO taps.

For the charging test at 4.2 K under the background field, we had two options: the positive current operation and negative current operation [17]. The positive current operation, where the current polarity for the test coil matches that of the background magnet, is more common but could lead to excessively high hoop strain and potential damage to the REBCO tape. Therefore, we opted for the negative current operation, where the current polarity for the test coil is opposite to that of the background magnet. In this case, the coil I_c is limited at the lower pancake disk, and it prevents excessive increases in hoop strain. The operating conditions for the negative current operation for each coil are summarized in Table II. The target current for the test coil is −1.2 kA, determined by the limit of the power supply, contributing 94% of the localized minimum I_c for the coil predicted by numerical simulation.

1) *CATT 1 results:* Fig. 10 shows the results of the negative current operation test for CATT 1. A sudden resistive voltage rise was observed around −690 A during current ramping. Consequently, the test coil was fully discharged without quench or thermal runaway.

Fig. 11 displays the measured voltage–current characteristic of CATT 1 in 77 K under the self-field before and after the CATT test, indicating noticeable decrease in coil performance.

After detaching CATT 1 from the test probe, buckling deformation was observed on the bottom surface of the coil, as shown in Fig. 12, whereas no visible deformation was noted on the top surface. The buckling was located at three positions on the bottom surface of the lower pancake disk. Similar deformation was also observed on the bottom surface of the upper pancake disk during unwinding. CATT 1 experienced degradation due to buckling deformation. Since delamination and microcracks in the REBCO layer were observed at this type of buckling, as reported in [6], we believe that this I_c reduction was caused by such failures in the REBCO layer.

Fig. 18 shows the measured longitudinal I_c distribution in 77 K before and after the CATT test. The measurements were performed at SuperPower using their Tapestar device. The "splice" denotes where tape lengths were soldered together for the Tapestar measurement. CATT 1 exhibited the maximum 80% I_c reduction. The I_c reduction is more significant closer to the inner diameter, with greater reductions observed in the lower disk compared to the upper disk.

2) *CATT 2 results:* In the case of CATT 2, a negative current operation test was not performed. The charging test result in 77 K (see Fig. 13), visual inspection and I_c measurement in longitudinal direction on REBCO tapes (see Fig. 18), showed

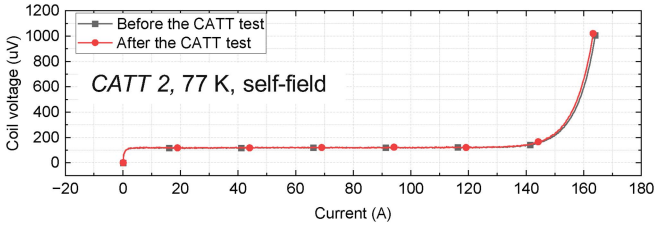

Fig. 13. Voltage-current curve of CATT 2 at 77 K under self-filed.

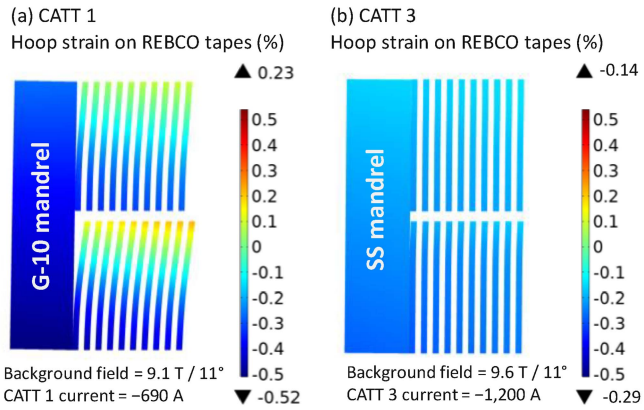

Fig. 14. Simulated distribution of hoop strain on REBCO tapes at (a) the timing of voltage rise with the CATT 1 current of −690 A during negative current operation in CATT 1 and (b) the CATT 3 current of −1200 A during negative current operation in CATT 3.

no degradation or deformation. Thus, CATT 2 withstood the combined axial pressure and SCIS, and the fatigue cycle.

3) *Cause of buckling in CATT 1:* Since the buckling in CATT 1 was found on the lower edge of the REBCO tapes, similar to the that reported in [6], this likely resulted from compressive hoop strain. The absence of degradation in CATT 2, despite similar conditions as shown in Tables I and II, suggests that the buckling in CATT 1 occurred during negative current operation. Fig. 14(a) displays the simulated hoop strain distribution on REBCO tapes at the time of voltage rise during the negative current operation in CATT 1. Although the magnitude of the minimum hoop strain was nearly same as that before charging the negative current, as shown in the Fig. 6(a), the area of compressive hoop strain is enlarged. This might have led to the observed buckling deformation. The simulation also shows that the magnitude and area of compressive hoop strain in the lower disk are greater than those in the upper disk, which corresponds to the longitudinal I_c measurement results in Fig. 18.

4) *CATT 3 results:* To reduce compressive hoop strain in CATT 3, we had changed mandrel material from G-10 to SS, which has significantly higher modulus than G-10. As shown in Fig. 15, no resistive voltage rise was observed during negative current operation up to −1.2 kA corresponding to 94% of the minimum I_c in the coil. The simulated hoop strain distribution on REBCO tapes at the test coil current of −1.2 kA is shown in Fig. 14(b), indicating the minimum hoop strain was suppressed to −0.29%. These experimental and simulation results

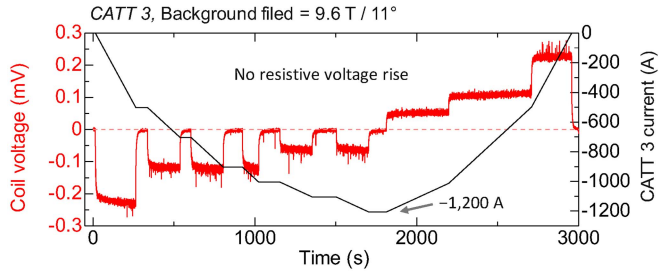

Fig. 15. Test results of negative current operation in CATT 3.

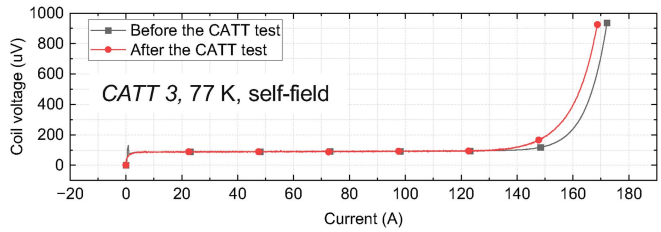

Fig. 16. Voltage-current curve of CATT 3 at 77 K under self-filed.

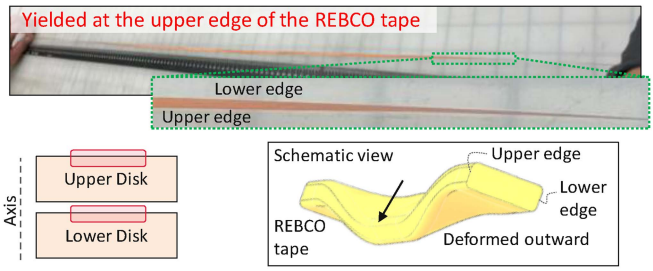

Fig. 17. Yielding found on CATT 3 after the test.

demonstrate that the SS mandrel effectively prevents buckling deformation by reducing compressive hoop strain.

However, the voltage–current characteristic of CATT 3 in 77 K, shown in Fig. 16, indicated a slight I_c decrease of 1.7%. Visual inspection revealed no visible deformation on the top and bottom surfaces of the coil, but yielding was observed at the upper edge of the REBCO tapes during unwinding, as shown in Fig. 17. This resembles the plastic deformation reported in [8], [10]. The measured longitudinal I_c distribution in Fig. 18 showed less than 14% I_c reduction, except for the locations where I_c reduction occurred due to handling during the unwinding process. Papers [8], [18] and [19] reported that such yielding can induce or propagate microcracks in the REBCO layer. We believe that the I_c reduction in CATT 3 is due to such failures in the REBCO layer.

We also believe this yielding and I_c reduction occurred due to the axial load of 170–180 kN applied during the initial increase. The nonlinear rise in measured hoop strain, shown in Fig. 8(c), may indicate yielding. Therefore, the degradation in CATT 3 was caused by excessive tensile hoop strain from combined axial load and SCIS.

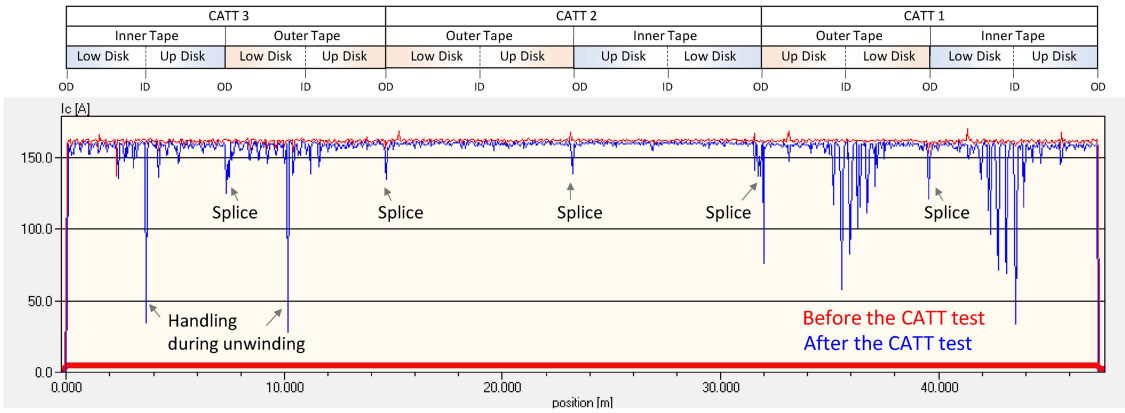

Fig. 18. The longitudinal I_c distribution in the REBCO tapes used for CATT coils measured in 77 K.

IV. Conclusion

We developed and conducted the combined axial pressure and tape tilting (CATT) test with three REBCO double pancake test coils (CATT 1, 2 and 3). In these tests, tape tilting was created by SCIS and axial pressure was applied mechanically by the actuator. The results showed that in CATT 3, a 50% of hoop strain enhancement occurred at 180 kN of axial load with 5.8° of estimated tilting angle, which led to yielding and I_c degradation in the REBCO tape. In CATT 1, although unrelated to axial pressure, buckling deformation resulted from compressive hoop strain during the negative current operation. We have also demonstrated that using a SS mandrel effectively prevents buckling deformation by reducing compressive hoop strain.

For future structural designs of ultra-high field REBCO coil, the relationship between tilting angle and axial pressure must be carefully managed, alongside the magnitude of compressive hoop strain.

As a perspective for the future study, as mentioned in Section I, axial pressure also provides friction forces, which suppress hoop strain in an actual magnet. Therefore, whether hoop strain is enhanced by axial pressure will depend on the balance between strain enhancement due to the CATT effect and strain reduction caused by friction. This needs further investigation. Additionally, the conditions under which buckling occurs, such as the magnitude and area of compressive hoop strain, remain unclear and should be clarified.

References

[1] Y. Li et al., "Magnetization and screening current in an 800 MHz (18.8 T) REBCO nuclear magnetic resonance insert magnet: Experimental results and numerical analysis," *Supercond. Sci. Technol.*, vol. 32, no. 10, 2019, Art. no. 105007, doi: 10.1088/1361-6668/ab3119.

[2] S. Hahn et al., "45.5-tesla direct-current magnetic field generated with a high-temperature superconducting magnet," *Nature*, vol. 570, pp. 496–499, 2019, doi: 10.1038/s41586-019-1293-1.

[3] Y. Yan et al., "Screening-current-induced mechanical strains in REBCO insert coils," *Supercond. Sci. Technol.*, vol. 34, no. 8, 2021, Art. no. 085012, doi: 10.1088/1361-6668/ac0b2d.

[4] Y. Yan, Y. Li, and T. Qu, "Screening current induced magnetic field and stress in ultra-high-field magnets using REBCO coated conductors," *Supercond. Sci. Technol.*, vol. 35, no. 1, 2022, Art. no. 014003, doi: 10.1088/1361-6668/ac392b.

[5] D. Kolb-Bond et al., "Screening current rotation effects: SCIF and strain in REBCO magnets," *Supercond. Sci. Technol.*, vol. 34, no. 9, 2021, Art. no. 095004, doi: 10.1088/1361-6668/ac1525.

[6] S. Takahashi et al., "Hoop stress modification, stress hysteresis and degradation of a REBCO coil due to the screening current under external magnetic field cycling," *IEEE Trans. Appl. Supercond.*, vol. 30, no. 4, Jun. 2020, Art. no. 4602607, doi: 10.1109/TASC.2020.2974837.

[7] H. Ueda et al., "Numerical evaluation of the deformation of REBCO pancake coil, considering winding tension, thermal stress, and screening-current-induced stress," *Supercond. Sci. Technol.*, vol. 34, no. 2, 2021, Art. no. 024003, doi: 10.1088/1361-6668/abcd24.

[8] J. Bang et al., "Elastic-plastic conductor damage evaluation at over 0.4% strain using a high-stress REBCO coil," *Supercond. Sci. Technol.*, vol. 37, 2024, Art. no. 095011, doi: 10.1088/1361-6668/ad6a9d.

[9] Y. Suetomi et al., "Screening current induced stress/strain analysis of high field REBCO coils with co-winding or over-banding reinforcement," *IEEE Trans. Appl. Supercond.*, vol. 34, no. 5, Aug. 2024, Art. no. 8400206, doi: 10.1109/TASC.2023.3342762.

[10] X. Hu et al., "Analyses of the plastic deformation of coated conductors deconstructed from ultra-high field test coils," *Supercond. Sci. Technol.*, vol. 33, no. 9, 2020, Art. no. 095012, doi: 10.1088/1361-6668/aba79d.

[11] Y. Nagasaki et al., "Axial compressive stress dependence of critical current of REBCO double-pancake coil," *IEEE Trans. Appl. Supercond.*, vol. 31, no. 5, Aug. 2021, Art. no. 8400405, doi: 10.1109/TASC.2021.3070119.

[12] S. Joshi, J. Cozzolino, R. Gupta, and W. Sampson, "Measurements of the effects of compressive loading on the narrow side of the HTS TAPE," *IEEE Trans. Appl. Supercond.*, vol. 30, no. 4, Jun. 2020, Art. no. 4600205, doi: 10.1109/TASC.2020.2966157.

[13] I. R. Dixon, E. S. Bosque, K. Buchholz, R. P. Walsh, and H. Bai, "REBCO coils with variable co-wind dimensions under static and cyclic axial pressure loads at 77 K," *IEEE Trans. Appl. Supercond.*, vol. 32, no. 6, Sep. 2022, Art. no. 4603204, doi: 10.1109/TASC.2022.3163084.

[14] J. Park, J. Bang, U. Bong, J. Kim, D. Abraimov, and S. Hahn, "Parametric study on effect of friction and overbanding in screening current stress of LBC magnet," *IEEE Trans. Appl. Supercond.*, vol. 31, no. 5, Aug. 2021, Art. no. 4603205, doi: 10.1109/TASC.2021.3070097.

[15] H. Kandel et al., "Sol-gel-derived $Al_2O_3-SiO_2$ composite coating for electrical insulation in HTS magnet technology," *IEEE Trans. Appl. Supercond.*, vol. 22, no. 5, Oct. 2012, Art. no. 7701605, doi: 10.1109/TASC.2012.2204745.

[16] J. Jaroszynski et al., "Rapid assessment of REBCO CC angular critical current density $J_c(B, T = 4.2\ \text{K}, \theta)$ using torque magnetometry up to at least 30 tesla," *Supercond. Sci. Technol.*, vol. 35, 2022, Art. no. 095009, doi: 10.1088/1361-6668/ac8318.

[17] E. Bosque et al., "Resolving the ic discrepancy between short samples and MTI coils within the 40 T Project at the NHMFL," in *Proc. MT-28 Int. Conf. Magnet Technol.*, 2023.

[18] Y. Zhou, D. Park, and Y. Iwasa, "Review of progress and challenges of key mechanical issues in high-field superconducting magnets," *Nat. Sci. Rev.*, vol. 10, no. 3, 2023, Art. no. nwad001, doi: 10.1093/nsr/nwad001.

[19] K. Kajita et al., "Degradation of a REBCO conductor due to an axial tensile stress under edgewise bending: A major stress mode of deterioration in a high field REBCO coil's performance," *Supercond. Sci. Technol.*, vol. 30, 2017, Art. no. 074002, doi: 10.1088/1361-6668/aa6c3.